THE 23RD CHESAPEAKE SAILING YACHT SYMPOSIUM
ANNAPOLIS, MARYLAND, MARCH 2019

6DOF behavior of an offshore racing trimaran in an unsteady environment

Paul Kerdraon[1], VPLP Design, Vannes, France, and Ecole Centrale Nantes, France
Boris Horel, Ecole Centrale Nantes, LHEEA res. dept. (ECN and CNRS), Nantes, France
Patrick Bot, Naval Academy Research Institute, Brest, France
Adrien Letourneur, VPLP Design, Vannes, France
David Le Touzé, Ecole Centrale Nantes, LHEEA res. dept. (ECN and CNRS), Nantes, France

ABSTRACT

While in recent years the use of hydrofoils has experienced a substantial growth, traditional design tools such as Velocity Prediction Programs (VPP) have proven inadequate to help architects and engineers with performance trade offs which now include specific stability issues related to these foils. The quest for performance also demands a better account of the unsteadiness of the environment in which the offshore yachts evolve.

Time-domain analysis and system-based modeling allow for an improved understanding of the controllability and dynamic stability of given geometries, enabling to adapt and refine the design. This paper presents such a dynamical unsteady model, based on the superposition of several loads components, computed from either numerical, empirical or analytical models. A test case and its results are presented to show the reliability and efficiency of the developed numerical tool, by comparing response amplitude operators of a reference hull form with experimental and numerical data.

Finally, the paper outlines two 6DOF dynamic simulations of an offshore trimaran. The first case shows a simple bear-away maneuver and compares two sail tuning strategies, while the second one presents the yacht evolution in unsteady wind demonstrating how in varying conditions the boat may reach attitudes that widely differ from the steady ones.

NOTATION

A	Wave amplitude
$\mathbf{A}$	Added mass coefficients matrix
$\mathbf{B}$	Damping coefficients matrix
Fn	Froude number
$\mathbf{F}_i$	Force component *i*
g	Acceleration of gravity
$\mathbf{I}$	Yacht inertia matrix
$\mathbf{K}$	Retardation function matrix
m	Yacht mass
$\mathbf{n}$	Outgoing body's normal vector
p_i	Pressure of incoming waves
S_w	Yacht wetted area
$\bar{U}$	Yacht mean speed
$\mathbf{V}$	Yacht linear velocity vector
δ_R	Rudder angle
$\boldsymbol{\xi}$	Ship perturbation vector
Φ_i	Potential of incoming waves
ρ	Water density
ω	Frequency-domain variable
	Wave circular frequency
$\boldsymbol{\omega}$	Yacht angular velocity vector

CFD	Computational Fluid Dynamics
DOF	Degree(s) of Freedom
DVPP	Dynamic Velocity Prediction Program
IMS	International Measurement System
RAO	Response Amplitude Operator
TWA	True Wind Angle
TWS	True Wind Speed
VPP	Velocity Prediction Program

[1] kerdraon@vannes.vplp.fr

INTRODUCTION

Velocity Prediction Programs are nowadays widely used in naval architecture offices to help architects and engineers in the design process of sailing yachts. Based on experimental, numerical or empirical data, they enable boats settings optimization to derive the reachable boat speeds in given steady conditions.
However, unlike inshore yachts such as the AC45 or the AC75, offshore vessels may encounter rough sea and wind conditions with short characteristic time of evolution. The study of the boat behavior in unsteady environment is therefore a key of the yacht real performance assessment and should be included in the design trade-offs.

In addition, recent years have seen a substantial growth of foiling technologies, leading to fully flying yachts and introducing specific stability issues with direct impact on speed. A better knowledge of the dynamic response of flying yachts is paramount for safe and sustained offshore flight. Non-linear couplings between the different degrees of freedom complicate further the study and traditional VPPs have proven inadequate to handle those matters with the accuracy required for high performance sailing.

In this context, numerical tools enabling time-domain analysis and including unsteady environment – often called Dynamic Velocity Prediction Programs (DVPPs) – have become a major research topic.

SAILING YACHT DYNAMIC SIMULATION

Ability to simulate maneuvers and especially tacking has long been the main subject of sailing dynamic studies (Keuning et al., 2005, Masuyama et al., 1995). In match racing, maneuvers are critical and simulations provide an efficient way for designers as well as crew to improve the on-water results (Binns et al., 2008). Most of those works are based on the usual maneuvering approach (Abkowitz, 1964) in which loads are described using hydrodynamic derivatives and enabling the modeling of the three or four degrees of freedom (DOFs) boat motion (surge, sway, yaw and sometimes roll). Nevertheless foiling greatly enhances the need to factor in the two other DOFs as heave (flight height) and trim (appendages angles of attack) are now at the core of boat stability (Heppel, 2015). Full 6 degrees of freedom modeling is therefore needed.

First works on adapting classical ship maneuvering theory to sailing yacht were undertaken in the late sixties, focusing mostly on steering and course stability. Introduction of time domain studies in the design of racing yachts occurred for the victorious 26th America's Cup challenger *Stars and Stripes* (see Oliver et al., 1987) using a quasi-steady approach. Based on the steady state models of the IMS VPP, Larsson (1990) and Ottosson et al. (2002) presented in the early nineties a four degrees of freedom simulator in which angular motions are accounted for by calculating induced velocities. Masuyama et al. (1993, 1995) developed a numerical tool based on hydrodynamic derivatives computed from tank tests and successfully compared their results to full scale measurements. A linear law was used to model the sail forces evolution at low apparent wind and simulate tacking maneuvers. Keuning et al. (2005) enlarged the possibilities and modularity of such tools by introducing the use of Delft Systematic Yacht Hull Series to compute the hydrodynamic coefficients. The same year, Richardt et al. (2005) proposed a full six degrees of freedom DVPP based on Masuyama's approach.

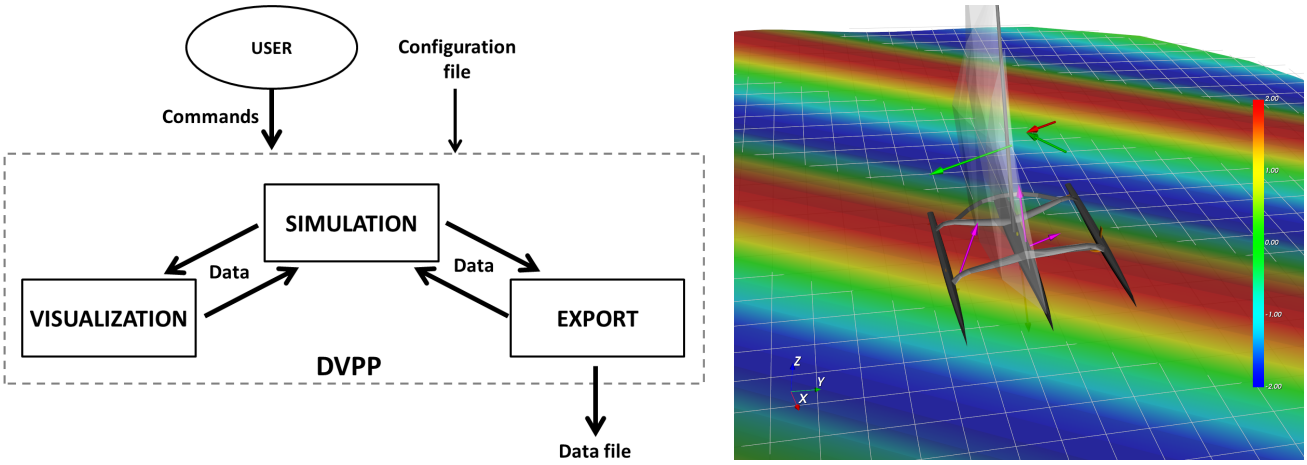

(a) Architecture.

(b) Visualization window.

Figure 1: Developed simulation tool.

Constant improvements of computational power have, on the other hand, opened the possibility to use CFD for time domain simulation by directly coupling the flow RANS solver with rigid body dynamic solvers (Jacquin et al., 2005, Lindstrand Levin and Larsson, 2017, Roux et al., 2008). Such approaches enable great accuracy while eliminating the need for empirical data or numerical pre-computations. The use of CFD as numerical VPP was achieved and work is now undertaken to add unsteady environment. Nevertheless, the computational time and costs of such techniques make them currently unavailable for naval architects when the comparison of several designs and configurations is needed.

System-based approaches, on the contrary, use empirical and theoretical models, experimental results or pre-computed numerical data to derive the hydrodynamic and aerodynamic loads and model the boat global behavior (Horel, 2016, 2017) with a computational efficiency that enables systematic studies, of appendages shapes and configurations for instance. Such a solution has therefore been selected and implemented (see Figure 1).

MATHEMATICAL MODELS OVERVIEW

Dynamics

The developed numerical tool is based on the resolution of the 6 degrees of freedom rigid body motion equations in the non inertial ship-fixed reference frame:

$$\begin{cases} m\left(\dfrac{d\mathbf{V}}{dt} + \boldsymbol{\omega} \wedge \mathbf{V}\right) = \mathbf{F} \\ \mathbf{I}\left(\dfrac{d\boldsymbol{\omega}}{dt} + \boldsymbol{\omega} \wedge \boldsymbol{\omega}\right) = \mathbf{M} \end{cases} \tag{1}$$

where $\mathbf{F}$, $\mathbf{M}$ are the external forces and moments and m, $\mathbf{I}$ the body mass and inertia.

The ship-fixed reference frame (X_b, Y_b, Z_b) is defined with X_b positive direction forwards, Y_b to port and Z_b upwards (see Figure 2). Its orientation with respect to the earth-fixed inertial reference frame (X_0, Y_0, Z_0) is expressed using the usual Cardan angle φ, θ, ψ (roll, pitch and yaw).

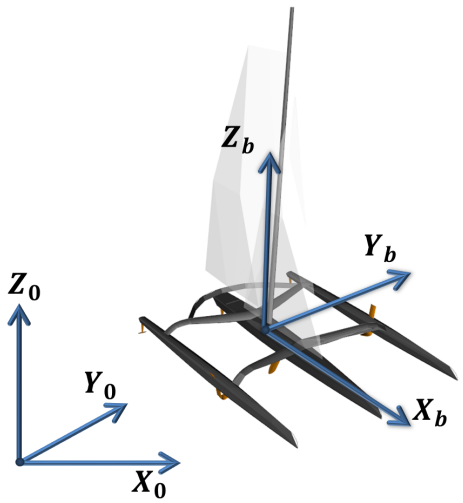

Figure 2: Coordinate systems definition.

Several explicit numerical integration schemes with various orders are available as well as adaptive time-stepping methods. External loads are given by the sum of all boat loaded components and can be divided in three main groups: hulls loads, appendages loads and aerodynamic loads.

Hulls loads

Hulls hydrodynamic loads are divided into low frequency (maneuvering) and high frequency (seakeeping: radiation and waves) loads, both are however expressed in the time domain.

• Maneuvering loads

Instead of the usual hydrodynamic derivatives approach (Abkowitz, 1964) for the maneuvering forces, the dynamic simulation tool uses polynomial response surfaces based on numerical viscous computations (RANS). The response surfaces are built on steady-state calculations for a wide range of hull attitudes, sinkages, leeway angles and speeds, which are then the input variables to the polynomial fit. It enables a full modeling of the six components of the hydrodynamic loads on each hull, including dependency to the boat possible changes of attitude and displacement due to the effect of appendages.

• Radiation force

The higher frequencies loads are based on the classical distinction between radiation, diffraction and Froude-Krylov forces. The former considers damping and added mass effects due to radiated waves generated by ship oscillations at the free surface. They are computed in the frequency domain using the Boundary Element Method (BEM) code Aquaplus (Delhommeau, 1993) developed at the Ecole Centrale de Nantes. Transformation of those frequency-domain coefficients to an impulse response function usable in the time-domain is carried out through Cummins equation (Cummins, 1962):

$$\begin{aligned}\mathbf{F}_{\mathrm{Rad}} = &- \mathbf{A}\left(\infty, \bar{U}\right)\ddot{\boldsymbol{\xi}} - \mathbf{B}\left(\infty, \bar{U}\right)\dot{\boldsymbol{\xi}} \\ &- \int_0^t \mathbf{K}\left(t-\tau, \bar{U}\right)\dot{\boldsymbol{\xi}}\left(\tau\right)d\tau\end{aligned} \tag{2}$$

where the retardation function $\mathbf{K}$ is given by the inverse Fourier transform of the frequency dependent damping component:

$$\mathbf{K}\left(t, \bar{U}\right) = \frac{2}{\pi}\int_0^\infty \left[\mathbf{B}\left(\omega, \bar{U}\right) - \mathbf{B}_\infty\left(\bar{U}\right)\right]\cos\left(\omega t\right)d\omega \tag{3}$$

• Wave loads

Diffraction loads are the first wave excitation force component. They originate in the reflection of the incident waves on the ship surface. Similarly, they are linearly modeled through the seakeeping code outputs, but directly using the frequency-domain expression :

$$\mathbf{F}_{\mathrm{DF}} = A\left|\mathbf{F_d}\right|(\omega_e)\,\cos\left(kX - \omega t + \varphi_{\mathbf{d}}(\omega_e)\right) \tag{4}$$

where $|\mathbf{F_d}|$ and $\varphi_{\mathbf{d}}$ are the modulus and phase of the diffraction force, X the ship abscissa along the wave propagation axis and ω_e the frequency of encounter given by:

$$\omega_e = \omega - \frac{\omega^2}{g}U\cos\mu \tag{5}$$

with μ the angle between the ship track and the wave propagation.

Finally, Froude-Krylov force gathers the loads of the incident wave pressure field p_i on the instantaneous ship wetted surface:

$$\mathbf{F}_{\mathrm{FK}} = -\iint_{S_w} p_i\,\mathbf{n}\,ds \tag{6}$$

where p_i is expressed through usual potential flow gravity waves theory:

$$p_i = -\rho\left[\frac{\partial\Phi_i}{\partial t} + \frac{1}{2}\left(\boldsymbol{\nabla}\Phi_i\right)^2\right] \tag{7}$$

While computing Froude-Krylov force, a correction of the hydrostatic loads to account for the deformation of the free surface is also performed.

Appendages loads

Appendages loads are in a first approach modeled using a Vortex Lattice Method with correction for viscous effects. Induced velocities, wave velocity field and appendages tuning angles are accounted for by computing effective angles between the appendage and the incoming flow following the Quasi-Steady Theory (QST) approach to compute the apparent flow velocity vector:

$$\mathbf{V}_{\mathbf{X}/\text{flow}} = \mathbf{V} + \boldsymbol{\omega} \wedge \mathbf{X} - \mathbf{V}^{\text{flow}} \tag{8}$$

where $\mathbf{X}$ is the coordinate vector of the considered location.

Hysteresis or fluid-structure interaction effects are neglected for the time being.

Aerodynamic loads

Similarly, the aerodynamic models are based on the usual Quasi-Steady Theory (QST) assumption (see Keuning et al., 2005, Richardt et al., 2005). Specifically, steady state sails polars are used while the apparent wind calculation accounts for the induced velocity due to the yacht angular motion. The IMS VPP (Claughton, 1999) approach that models sails de-powering through the *Flat* (sail lift reduction) and *Twist* (center of effort lowering) parameters is used.

A correction is added to model the aerodynamic inertia provided by the sails through the method described in Gerhardt et al. (2009). The sails added mass is approximated using a strip theory approach and integrating the potential flow expression of the added mass of an infinitely long, flat plate along the sail surface. The work of Tuckerman [1926] is used to derive a three-dimensional effect factor that proved rather consistent when compared to experimental measurements on a model sail by Gerhardt et al..

As was shown by Augier et al. (2013) and Fossati and Muggiasca (2011), such simple models do not reproduce fully the unsteady aerodynamic behavior of sails, and especially hysteresis phenomena. Research still needs to be carried out to integrate such aspects in DVPPs.

Control systems

Class rules on yacht control systems are a key issue in the future of high-performance sailing, especially offshore. Sportsmanship, human safety, energy consumption, financial costs are intimately linked to the decision to authorize them on board. For the time being, the Ultim Class 32/23 does not allow control system other than the helm autopilot. As this paper is concerned with the simulation of an offshore trimaran complying with those class rules, no control system of foils or centerboard is enabled and therefore no control of heel, pitch or ride-height. Unlike dinghies, Moths or America's Cup catamarans, Ultim trimarans take advantage of their substantial inertia which enable them to go through (limited) changes of the environmental conditions, wind gusts for instance, without immediate capsize.

The autopilot is an usual proportional-derivative controller:

$$\delta_R = K_p \left(\psi - \psi_T\right) + K_p T_D \dot{\psi} \tag{9}$$

where

δ_R rudder angle,
ψ_T targeted heading,
$\psi, \dot{\psi}$ yacht heading and its first order derivative,
K_p controller proportional coefficient,
T_D controller derivative coefficient.

The coefficients used in this paper have been manually tuned on a one degree of freedom (yaw) test simulation. To this end, T_D is first set to zero and K_p adjusted by finding a compromise between the system's stability and settling time. Second, T_D is increased to reduce oscillations while avoiding excessive overshoots and instability.

VALIDATION: HEAVE AND PITCH OSCILLATIONS OF WIGLEY III IN WAVES

Case presentation

This test case is built on the study of four Wigleys in regular head waves by Journée (1992). Wigleys are fully parametric and mathematically defined hull forms. The presented work focuses on Wigley III. Its body plan and characteristics are respectively given in Figure 3 and Table 1.

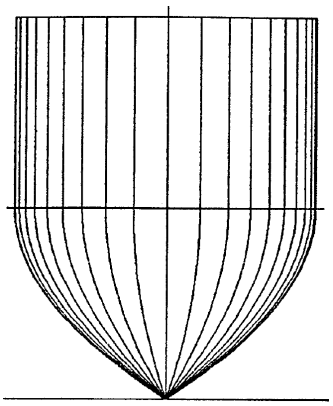

Figure 3: Wigley III body plan.

Length L	$3.0\,\mathrm{m}$
Breadth B	$0.3\,\mathrm{m}$
Amidship section coefficient C_m	0.667
Draft d	$0.1875\,\mathrm{m}$
Displacement ∇	$0.078\,\mathrm{m}^3$
Pitch radius of inertia k_{yy}	$0.75\,\mathrm{m}$
Center of rotation above base $\mathbf{KR}$	$0.1875\,\mathrm{m}$
Center of gravity above base $\mathbf{KG}$	$0.1700\,\mathrm{m}$

Table 1: Wigley III dimensions.

In his paper, Journée presents experimental results from tank testing at the Shiphydromechanics Laboratory of the Delft University of Technology as well as numerical ones computed through the 6 degrees of freedom program SEAWAY that implements both ordinary and modified strip theory methods. Hydrodynamic coefficients, wave loads, heave and pitch motions as well as added resistance results are presented.

Results

In the purpose of validation, results from the developed dynamic simulation tool are compared to the reference values provided by Journée. Simulations are run using the models previously presented. Infinite depth Airy waves are used, while one wave amplitude, $A = 0.02\,\mathrm{m}$, and four Froude numbers, 0, 0.2, 0.3 and 0.4, are considered.

The heave and pitch response amplitude operators are defined as:

$$\mathrm{RAO}_z\left(\omega\right) = \frac{z\left(\omega\right)}{A} \tag{10a}$$

$$\mathrm{RAO}_\theta\left(\omega\right) = \frac{\theta\left(\omega\right) L}{2\pi A} \tag{10b}$$

where z and θ are the heave and pitch response.

The moduli of the response amplitude operators for $Fn = 0$ are presented in Figure 4. The results correlate almost perfectly with both experimental and numerical results. The pitch motion peak is slightly lower than Journée's experimental data but is in excellent agreement with his own numerical results. Both low and high frequencies limits are consistent.

As the speed increases, a resonance peak of increasing intensity appears in both heave and pitch motions. The overall response and the peak position are rather well described, especially in pitch. The heave response shows however an underestimated resonance peak intensity. This discrepancy is due to the moderate quality of the speed dependency modeling of radiation and diffraction loads, which are here critical to properly track the resonance. In addition, the considered Froude numbers of the reference paper are relatively small compared to the usual values seen by high performance sailing yachts. For those reasons, tank tests have been planned to improve and validate our models in this regard.

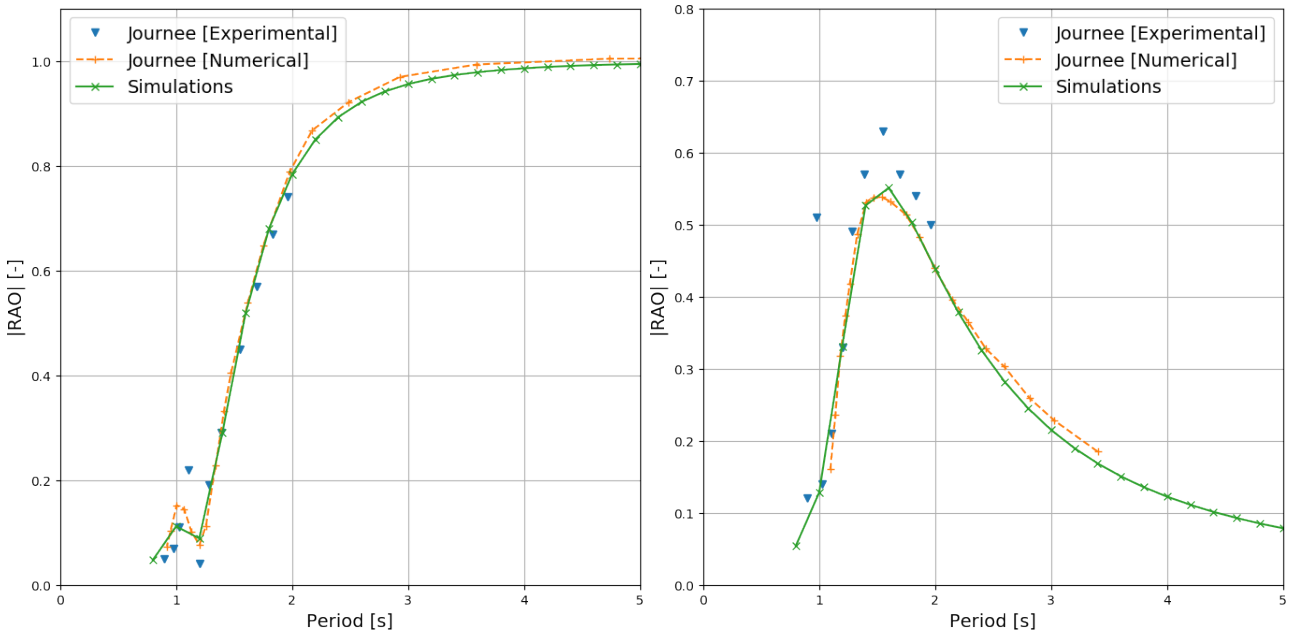

(a) Heave motion.

(b) Pitch motion.

Figure 4: Wigley III response amplitude operators at $Fn = 0$.

OFFSHORE TRIMARAN SIMULATIONS

Considered yacht

This part presents two simulations examples which underline specificities and interests of dynamic studies compared to steady ones. The simulated yacht is *Macif 100*, an offshore trimaran of the Ultim class. Skippered by François Gabart, she has been the holder of the single handed sailing around-the-world record since 2017 (in 42 days 16 hours 40 minutes 35 seconds). Those simulations consider the appendages set that was used for the circumnavigation: two small L-foils, one centerboard and three T-rudders (one on each hull).

Length L	30.0 m
Breadth B	21.0 m
Max. draft D	4.5 m
Air draft H	35.0 m
Displacement m	14.5 t
Launched	2015
Architect	VPLP
Shipyard	CDK Technologies

From *www.macifcourseaulargе.com/trimaran-macif/bateau/.*

Table 2: *Macif 100* characteristics.

Simple maneuver

As known by VPP engineers, a given configuration may lead to different equilibrium states (and thus different boat speeds), especially when the yacht has the ability to evolve in different modes (archimedean, fully flying, hybrid). The aim of this first simulation is to illustrate this specificity by comparing two sail trimming strategies and showing that even though the final configuration is the same in both cases, the final state largely differs, with a substantial speed delta.

Flat water conditions are considered and the yacht initially evolves upwind in 19 knots of wind at $50°$ True Wind Angle on port tack. The simulation is carried out in six degrees of freedom, with only an autopilot for the rudder angle. At $t = 50\,\text{s}$, the target heading is increased by sixty degrees so that the yacht bears away (see Figure 5). No change of sail is allowed.

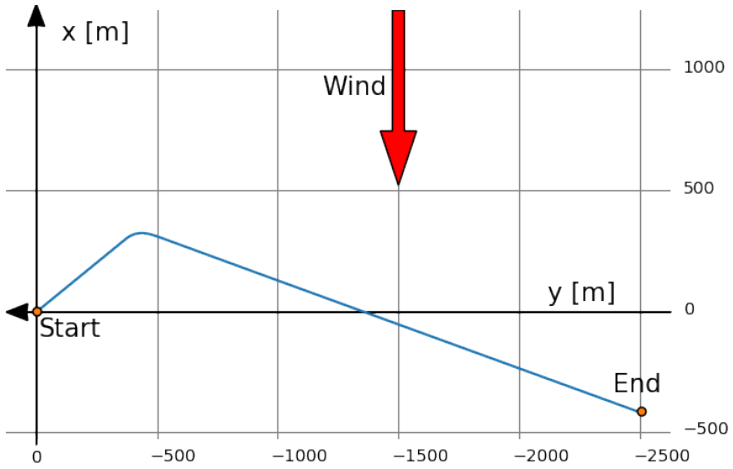

Figure 5: Yacht trajectory during the maneuver.

Initial and final states optimal configurations are known from steady VPP studies (board extension, rudder rake, *Flat* and *Twist*, etc.)., which show that in the final situation steady state optimal configuration sails must be depowered (twisted). The compared strategies focus on the timing of specific action: in the first one, this trimming is operated progressively, but directly after the rudder action, while in the second one, the sails are twisted only after the main hull has exited the water.

An important bias of the aerodynamic model must here be underlined. Steady state polars provide, for each wind angles, the lift and drag coefficients of the sails when optimally trimmed. Also, when used in dynamic situations, using such polars is equivalent to making the assumption that the sails are optimally trimmed at the same speed as the apparent wind angle increases. The strategies compared here only consider the sails twist, which enables the lowering of the center of effort at the cost of an increased drag coefficient. But in both cases, the aerodynamic model considers that the sheets are eased as the yacht bears away.

With the second strategy the yacht maintains a strong heeling moment which makes her heel and decreases the dynamic displacement of the main hull. The yacht can then accelerate, increasing thus the lift force of the foil in a virtuous circle that sees the hulls dynamic buoyancy and drag replaced by the foil action. Finally, the sails need to be twisted to enable the heeling moment to be balanced (as the boat accelerates, the aerodynamic heeling moment keeps on increasing otherwise). Acting too soon, as in the first strategy, prevents the yacht, under-powered, from lifting the main hull (Figure 6c), with an implicated lack of speed of more than 4.5 knots (Figure 6a).

Pushed by the inertial forces after the start of the turn, the yacht keeps briefly a non negligible speed component in the direction of her initial motion, that is to windward. This explains the negative leeway peak shown in Figure 6b.
The ratio of the main hull wetted surface area to its nominal value is shown in Figure 6f. Its evolution is close to the heel angle behavior and, while it is blocked at about 25% when using the first strategy, it indeed tends to zero in the second case.
The pitch angle evolution is visible in Figure 6g. Its evolution is driven by two main phenomena. First, after the maneuver, the speeds are globally higher in both strategies. As the speed increases, the aerodynamic pitching moment increases, leading to a greater pitch angle (bow down). However, another aspect is at stake in the second strategy: the main hull leaves the water and its pitching moment component cancels out. That is why the second boat shows a lower pitch angle than the first one.

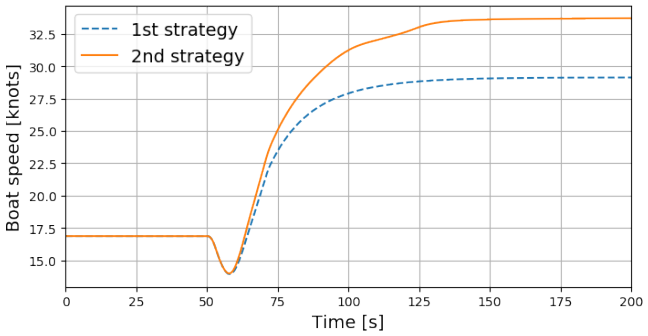

(a) Boat speed.

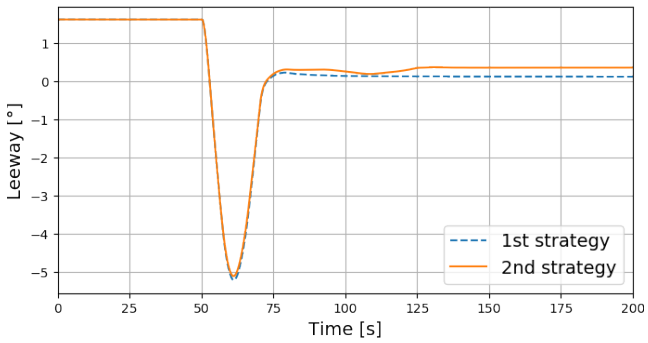

(b) Leeway angle.

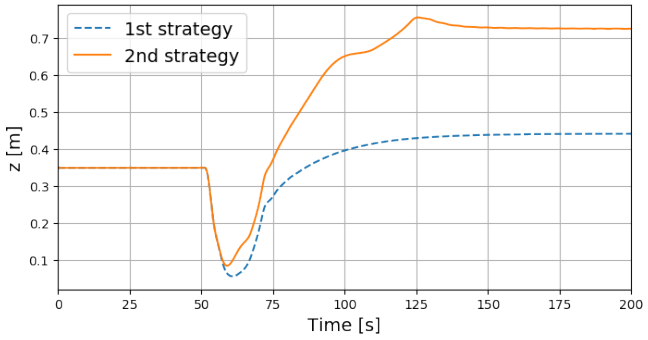

(c) Main hull reference point altitude.

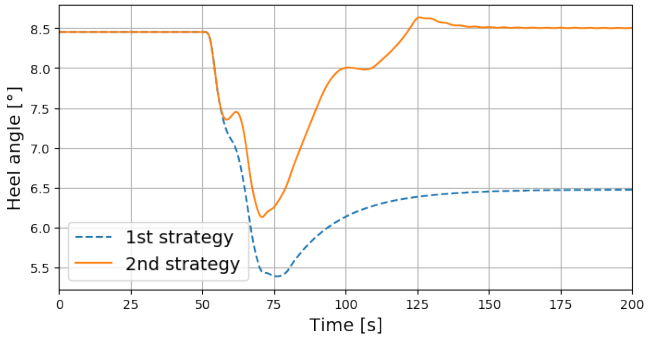

(d) Heel angle.

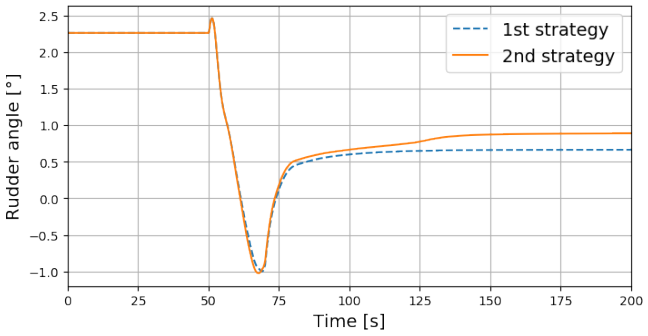

(e) Rudder angle.

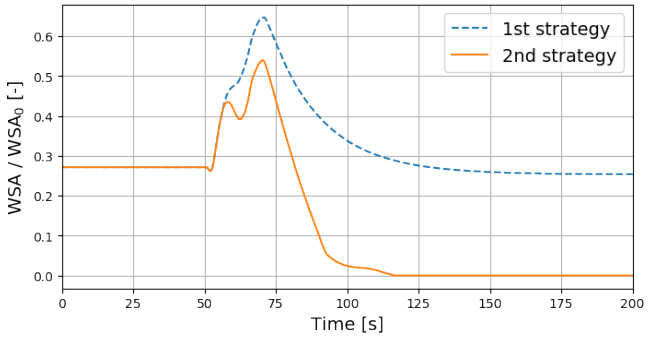

(f) Relative value of main hull wetted surface area.

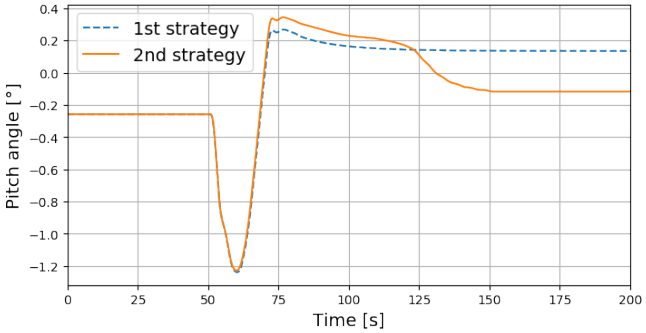

(g) Pitch angle (positive bow down).

Figure 6: Comparison of the two trimming strategies.

Behavior in unsteady wind conditions

This second simulation case aims at showing the interest of dynamic studies to predict potentially critical situations when evolving in unsteady conditions. The consequences on the yacht behavior of an irregular wind are studied. Unsteadiness is modeled by adding harmonic components to the mean True Wind Direction TWD_0 while the True Wind Speed is kept constant at 18 knots:

$$\mathrm{TWD}\,(t) = \mathrm{TWD}_0 \left[1 + \sum_i k_i \sin\left(\frac{2\pi}{T_i} t\right)\right] \tag{11}$$

The periods T_i and the intensity factors k_i of the chosen harmonic components are given in Table 3. Periods are chosen so that they are not multiples of each other, in order to increase the time necessary to observe a periodic behavior. Time evolution of the True Wind Direction is visible in Figure 7.

i	Period [s]	Frequency [Hz]	Intensity factor
1	41	0.0244	0.04
2	17	0.0588	0.03
3	7	0.143	0.02
4	6.5	0.154	0.005
5	5	0.200	0.01

Table 3: Wind harmonic components.

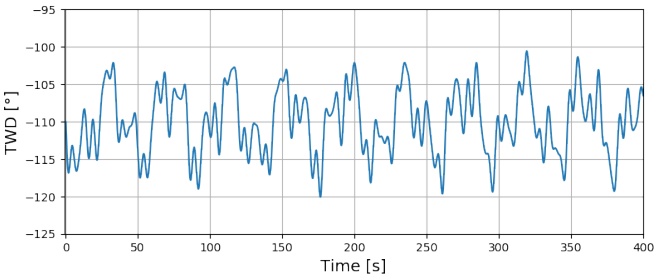

Figure 7: True Wind Direction evolution.

The boat is released from a VPP optimized equilibrium corresponding to TWA 110° / TWS 18 kn at $t = 0$. It is interesting to notice that, in such a configuration the boat speed is about 30 knots, and therefore a major component of the apparent wind. Fluctuations are thus much smaller in apparent wind than in true wind. During the 400 s simulation the standard deviation of the True Wind Direction is 4.3° and the amplitude between its extrema is 19.5°, the corresponding measures for the Apparent Wind Angle give respectively 1.4° and 6.1°. Some of the simulation outputs are shown in Figure 8. The yacht is free to evolve in 6 degrees of freedom, while an autopilot with a constant heading target ($\psi_T = 0°$) controls the rudders.

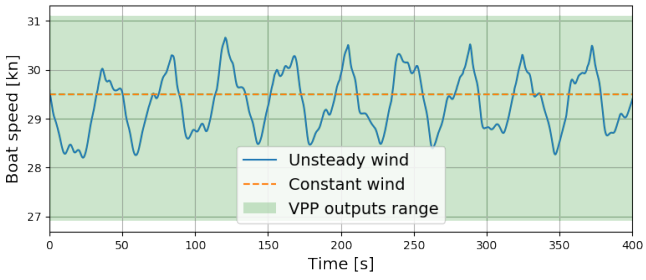

(a) Boat speed.

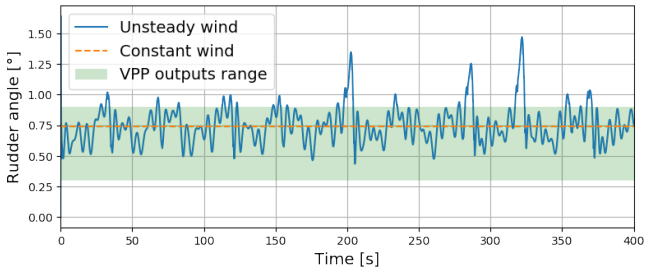

(b) Rudder angle.

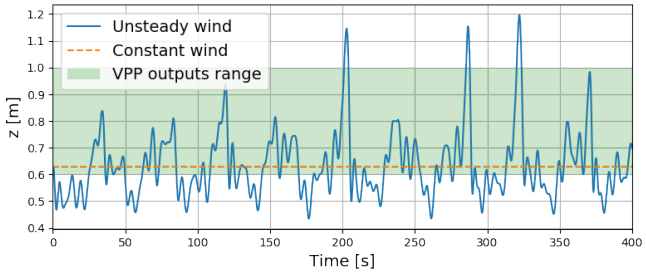

(c) Main hull reference point altitude.

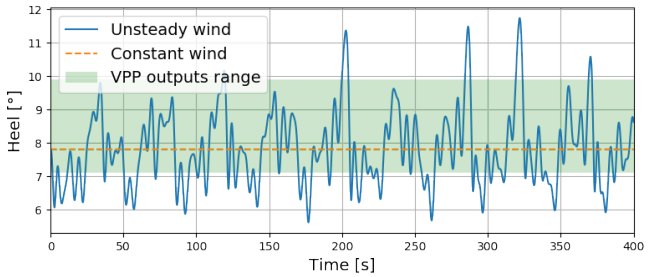

(d) Heel angle.

Figure 8: Dynamic simulation results compared to steady VPP optimization on the same True Wind Angle range.

One can notice three peaks where the heel angle almost reaches $12°$. Similar peaks are also visible on the altitude response. Consistently, Figure 7 shows that they correspond to situations where the wind heads (TWD maxima as the yacht heads North on port tack). However, such values of the True Wind Angle are reached several times without resulting in such situations. This demonstrates how the wind sequence has a strong impact on the yacht instantaneous behavior and proves how necessary time-domain simulations are for the complete understanding of the yacht behavior.

Similarly, Figure 8 shows in green the limits reached in a steady VPP when the yacht configuration is kept constant and the True Wind Angle ranges from $100°$ to $120°$, the minimal and maximal values of Figure 7. From time to time those values are largely exceeded. This shows, as could be expected, that steady state analysis can hide critical situations. On the contrary, the simulated boat speed is well contained within the VPP limits, as the wind oscillates too quickly for the speed to settle to the steady equilibrium values seen in VPP. The average speed during the simulated sequence is 29.3 knots, which is slightly below the speed reached in steady wind (29.5 knots).

Unlike the other outputs, the boat speed presents a low frequency harmonic strongly dominating the high frequency ones. This can be explained by the loads' dependency to the boat speed that tends to damp the response and by the low-pass filtering due to the yacht inertia, that filters the high frequency components of the excitation signal. This can be verified by comparing the power spectral densities of the output signals with the input one (Figure 9), which consistently shows that the first harmonic of the speed PSD is largely dominant over the other components. On the contrary, the linear and angular positions signals show a spectrum that is relatively close to the input one, with some additional very small harmonics. The fourth component being rather weak and close to the third one, it is hardly distinguishable in the shown spectra.

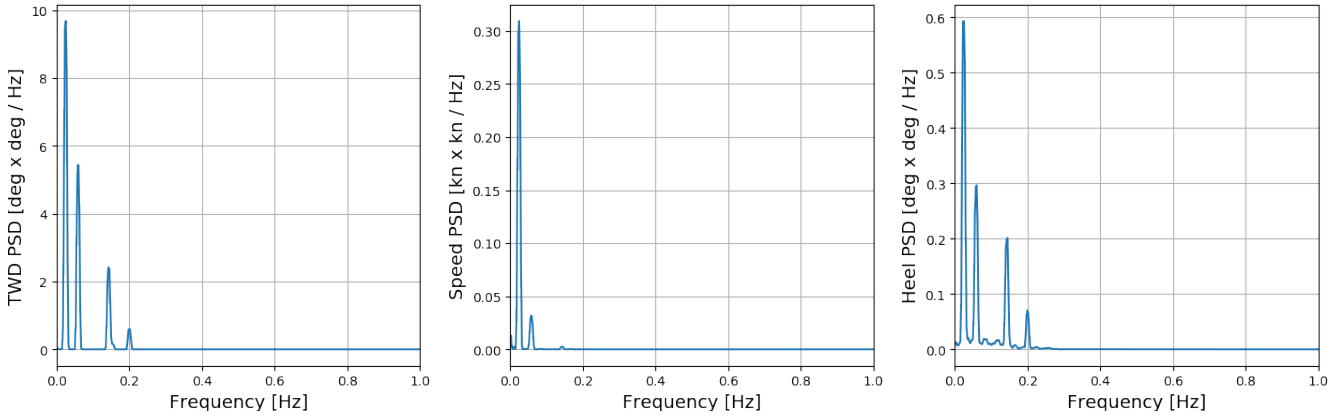

(a) Input signal: True Wind Direction (b) Output signal: Speed (c) Output signal: Heel angle

Figure 9: Power spectral densities of the input and outputs signals showing the boat speed low-pass filtering.

CONCLUSION

This paper describes the development and models of a numerical tool for sailing yacht dynamic behavior analysis. Validation case on a Wigley III hull shows encouraging consistent results for the heave and pitch response in waves. Preliminary simulations are presented to demonstrate the DVPP abilities, especially to study dynamic situations in which the yacht attitudes heavily differ from the corresponding steady state ones. In particular, it is shown how for identical values of the wind angle it is possible to observe highly different attitudes depending on the recent history of the yacht and her environment. The example cases also show the sensibility of the yacht behavior to the tuning strategies, and the necessity for the user to find a tuning path to the VPP optimized boat speed.

Such a numerical tool therefore brings a relevant help to yacht designers and sailors in order to predict and identify critical situations where the dynamic stability and performances of the yacht can be affected.

Work is however still needed, especially regarding appendages and aerodynamic loads, to handle a wider range of dynamic situations. Tuning strategies and appendages control are also major issues to be able to pilot the boat optimally.

PERSPECTIVES

Future work will aim at improving the previously mentioned points. Model tests in the towing tank facility of the LHEEA laboratory are also planned to improve the transient loads modeling of hulls and appendages. Such experiments will also enable to validate additional aspects of the implemented dynamic models.

ACKNOWLEDGMENTS

This work is supported and funded by VPLP Design and the ANRT (National Association for Research and Technology).

REFERENCES

M. A. Abkowitz. Lectures on ship hydrodynamics - Steering and manoeuvrability. Report no. hy-5, Hydrodynamics Department, Hydro- and Aerodynamics Laboratory, Lyngby, Denmark, May 1964.

B. Augier, P. Bot, F. Hauville, and M. Durand. Dynamic behaviour of a flexible yacht sail plan. *Ocean Engineering*, 66: 32–43, 2013.

J. R. Binns, K. Hochkirch, F. De Bord, and I. A. Burns. The development and use of sailing simulation for IACC starting manoeuvre training. In *3rd High Performance Yacht Design Conference*, pages 158–167, Auckland, New Zealand, 2008.

A. Claughton. Developments in the IMS VPP formulation. In *The 14th Chesapeake Sailing Yacht Symposium*, Annapolis, MD, USA, 1999.

W. E. Cummins. The impulse response function and ship motion. Report 1661, Navy Department, David Taylor Model Basin – Hydromechanics Laboratory, MD, USA, 1962.

G. Delhommeau. Seakeeping codes Aquadyn and Aquaplus. In *19th WEGEMT School on Numerical Simulation of Hydrodynamics: Ships and Offshore Structures*, Nantes, France, Sept. 1993.

F. Fossati and S. Muggiasca. Experimental investigation of sail aerodynamic behavior in dynamic conditions. *Journal of Sailboat Technology*, 2011.

F. C. Gerhardt, D. Le Pelley, R. Flay, and P. Richards. Tacking in the wind tunnel. In *The 19th Chesapeake Sailing Yacht Symposium*, pages 161–175, Annapolis, MD, USA, Mar. 2009.

P. Heppel. Flight dynamics of sailing foilers. In *5th High Performance Yacht Design Conference*, pages 180–189, Auckland, New Zealand, 2015.

B. Horel. *Modélisation physique du comportement du navire par mer de l'arrière*. PhD thesis, Ecole centrale de Nantes, France, 2016.

B. Horel. System-based modeling of a foiling catamaran. In *The 4th International Conference on Innovation in High Performance Sailing Yachts*, Lorient, France, 2017.

E. Jacquin, P.-E. Guillerm, Q. Derbanne, L. Boudet, and B. Alessandrini. Simulation d'essais d'extinction et de roulis forcé à l'aide d'un code de calcul Navier-Stokes à surface libre instationnaire. In *10èmes Journées de l'Hydrodynamique*, Nantes, France, Mar. 2005.

J. M. J. Journée. Experiments and calculations on 4 Wigley hull forms in head waves. Report 0909, Ship Hydromechanics Laboratory, Delft University of Technology, Delft, The Netherlands, May 1992.

J. A. Keuning, K. J. Vermeulen, and E. J. De Ridder. A generic mathematical model for the maneuvering and tacking of a sailing yacht. In *The 17th Chesapeake Sailing Yacht Symposium*, pages 143–163, Annapolis, MD, USA, Mar. 2005.

L. Larsson. Scientific methods in yacht design. *Annual Review of Fluid Mechanics*, 22(1):349–385, 1990.

R. Lindstrand Levin and L. Larsson. Sailing yacht performance prediction based on coupled CFD and rigid body dynamics in 6 degrees of freedom. *Ocean Engineering*, 144:362–373, 2017.

Y. Masuyama, I. Nakamura, H. Tatano, and K. Takagi. Dynamic performance of sailing cruiser by full-scale sea tests. In *The 11th Chesapeake Sailing Yacht Symposium*, pages 161–179, Annapolis, MD, USA, Jan. 1993.

Y. Masuyama, T. Fukasawa, and H. Sasagawa. Tacking simulation of sailing yachts–numerical integration of equations of motion and application of neural network technique. In *The 12th Chesapeake Sailing Yacht Symposium*, Annapolis, USA, 1995.

J. C. Oliver, J. S. Letcher, Jr., and N. Salvesen. Performance predictions for Stars & Stripes. In *Transactions Society of Naval Architects and Marine Engineers*, volume 95, pages 239–261, New York, NY, USA, Nov. 1987.

P. Ottosson, M. Brown, and L. Larsson. The effect of pitch radius of gyration on sailing yacht performance. In *High Performance Yacht Design Conference*, Auckland, New-Zealand, Dec. 2002.

T. Richardt, S. Harries, and K. Hochkirch. Maneuvering simulations for ships and sailing yachts using Friendship-Equilibrium as an open modular workbench. In *International EuroConference on Computer Applications and Information Technology in the Maritime Industries, COMPIT*, pages 101–115, Hamburg, Germany, May 2005.

Y. Roux, M. Durand, A. Leroyer, P. Queutey, M. Visonneau, J. Raymond, J.-M. Finot, F. Hauville, and A. Purwanto. Strongly coupled VPP and CFD RANSE code for sailing yacht performance prediction. In *3rd High Performance Yacht Design Conference*, pages 215–226, Auckland, New Zealand, 2008.